Rayleigh and Brillouin scattering for binary systems of several organic liquids

1994 J. Phys.: Condens. Matter 6 339

(http://iopscience.iop.org/0953-8984/6/2/006)

J. Phys.: Condens. Matter 6 (1994) 339–350. Printed in the UK

Rayleigh and Brillouin scattering for binary systems of several organic liquids

S Kawase†, K Maruyama‡ and H Okazaki§

† College of Biomedical Technology, Niigata University, Asahimachi-dori, Niigata 951, Japan
‡ Graduate School of Science and Technology, Niigata University, Igarashi, Niigata 950-21, Japan
§ College of General Education, Niigata University, Igarashi, Niigata 950-21, Japan

Received 3 August 1993, in final form 17 September 1993

Abstract. Rayleigh and Brillouin scattering have been investigated for organic–organic liquid mixtures. For conformal liquid mixtures (CS_2–$CHCl_3$ and C_6H_6–CH_3OH systems), the Rayleigh scattering intensity and the adiabatic compressibility derived from the Brillouin shift are well expressed by the regular solution model, slightly changing the interaction parameter as a function of the concentration. The half widths of the Brillouin peaks show different tendencies with concentration for these two systems. For the C_6H_{12}–CH_3OH system, the scattering intensity varies as expected from the phase diagram, although it has a miscibility gap.

1. Introduction

Since the discovery of critical opalescence in a binary fluid system, the experimental technique of Rayleigh and Brillouin scattering has given us plenty of information in terms of macroscopic data, for example, isothermal compressibility [1], acoustic relaxation [2] and glass transition [3, 4]. On the other hand, the relations between thermodynamic properties of mixing and microscopic fluctuations in binary fluids have been derived by Bhatia and Thornton [5], based on the grand partition function in the theory of statistical mechanics (hereafter this will be referred to as BT theory). Therefore the critical opalescence phenomena can also be analysed in terms of BT theory. In relation to the BT theory, the excess free energy [6], the interaction parameter [7, 8] and the associated complex formation [9] of liquid mixtures have been investigated using light scattering measurements.

Under these circumstances, we have tried to measure the Rayleigh and Brillouin scattering for several binary mixtures of organic fluids, because some of them are conformal and another has a tendence to phase separation. In this paper we report new results of Rayleigh and Brillouin scattering measurements for CS_2–$CHCl_3$, C_6H_6–CH_3OH and C_6H_{12}–CH_3OH systems.

2. Experimental details

Figure 1 shows a block diagram of the system for measuring the Rayleigh and Brillouin scattering intensities. The instrument consists of a single-mode argon-ion laser (NEC, GLG3460), a Fabry–Pérot interferometer (Mizojiri, FP-T30), a lock-in amplifier (NF, LI-570A), and an X–Y recorder (Riken Denshi F-5C). The exciting-light wavelength was

0953-8984/94/020339+12$07.50

514.5 nm and the laser power was about 500 mW. The incident light power was adjusted by ND filters and was monitored with a solar cell. The light beam was chopped at 225 Hz and focused at the centre of a sample cell by a lens L_1 (focal length $f_1 = 3$ cm). The size of the glass sample cell was 12ϕ (outer diameter) $\times$ 32 mm (height), and it had a screw cap. The light scattered at right angles was focused by a lens L_2 (focal length $f_2 = 25$ cm) onto a slit (slit width 0.5 mm) of a monochromator. The light passing through the monochromator with a resolution of 2.8 nm was made parallel by a lens L_3 (focal length $f_3 = 20$ cm), and analysed by the Fabry-Pérot interferometer. The spacer between the interferometer etalons has a thickness of 6.030 mm, giving a free spectral range of 0.829 cm^{-1}, and an overall instrumental half-width of about 0.015 cm^{-1}, varying slightly for different alignments. The interferometer was pressure scanned by supplying nitrogen gas to the chamber enclosing the etalons. The interferometer output was focused onto a screen by a lens L_4 (focal length $f_4 = 30$ cm). The light passing through a pinhole (diameter = 0.3 mm) on the screen was detected by a photomultiplier tube (Hamamatsu Photonics, R647-04). The output current from the tube was led into the lock-in amplifier. The time constant of the lock-in amplifier was chosen as 0.3 s, which was found to be sufficient for obtaining good S/N ratio but was not long enough to distort the line shape. The reference signal to the lock-in amplifier was synchronized with the light chopper. The output of the lock-in amplifier was indicated on the X–Y recorder. The X-axis of the recorder was supplied from the pressure transducer of the interferometer to the voltage.

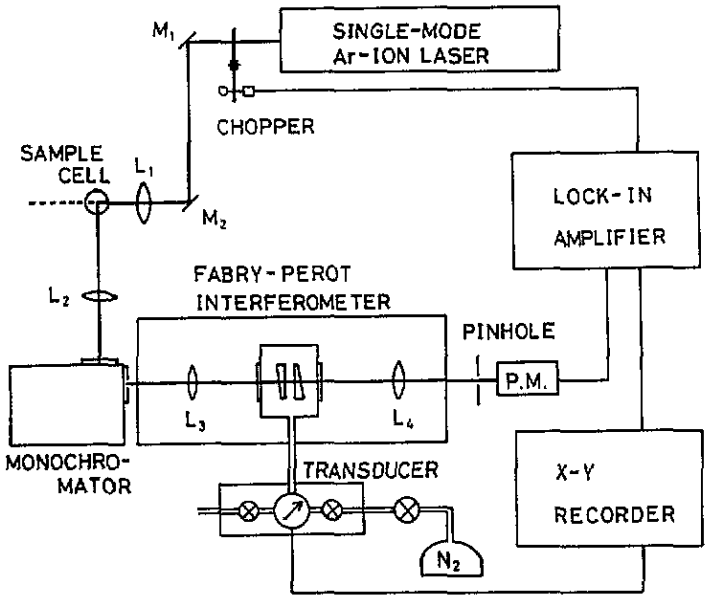

Figure 1. A block diagram of the system for measuring the Rayleigh and Brillouin scattering. M_1 and M_2 are mirrors; L_1, L_2, L_3, and L_4 are lenses; ⊗ are valves.

The samples used in this experiment were commercially available reagents. They were made dust free by using a membrane filter (Advantec, Dismic) with a pore size of 0.2 μm. The test of a solution being dust free was performed by comparing the observed Rayleigh intensity with the true Rayleigh intensity of dust-free samples, which was essentially similar

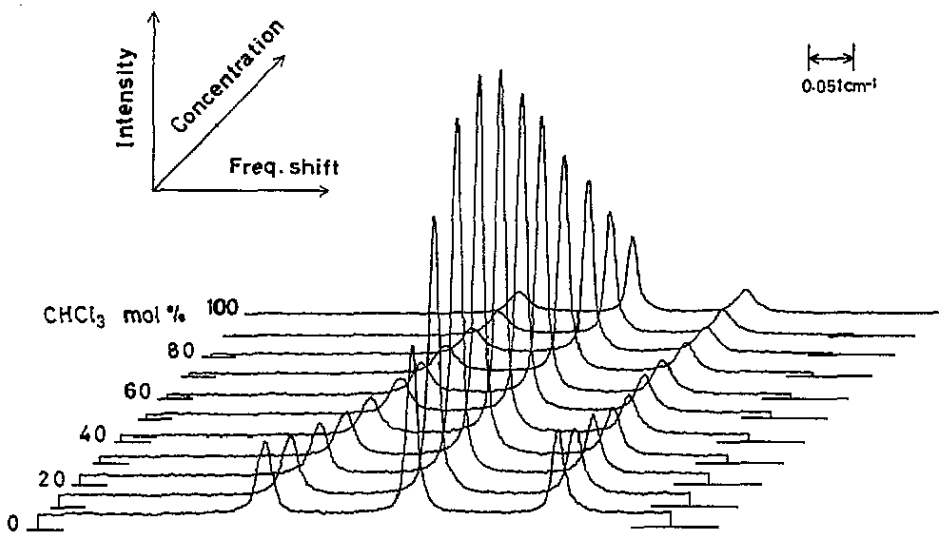

Figure 2. The observed light-scattering spectra of CS_2–$CHCl_3$ mixtures and their variation with changing composition. The horizontal bars at each side of the spectra represent the base line. The molar fraction of $CHCl_3$ is indicated in the figure.

to that described by Iwasaki *et al* [10]. We can determine that mixture samples are dust free by the same method as applied for pure liquids.

The observed light-scattering spectra for the CS_2–$CHCl_3$ system as typical examples are shown in figure 2. It may be seen from this figure that the intensities of the Rayleigh lines increase remarkably on passing from pure liquids to binary solutions. The intensity change in the Brillouin lines is quite different from that of the Rayleigh lines. The background intensity due to a Rayleigh wing is large for pure CS_2 and almost zero for pure $CHCl_3$. The experimental curves were well described by the sum of Lorentzian curves and therefore it was easy to separate the Rayleigh peak and the Brillouin doublet.

The sample temperature was kept at 25 °C within an accuracy of 0.5 °C during the course of the measurements.

3. Theoretical background

By analogy with Van Hove's neutron-scattering formalism [11], and following Komarov and Fisher [12], the intensity $I(R, \omega)$ of light scattered from a pure fluid, per unit incident intensity, per unit solid angle, per unit frequency range ω, we have derived the following expression [13]:

$$I(R, \omega) = \left(\frac{N\alpha_e^2\Omega_0^4}{2\pi R^2 c^4}\right) \sin^2\varphi S(q, \omega) \tag{1}$$

where N is the number of molecules in the fluid, α_e an effective polarizability per molecule, Ω_0 the angular frequency of incident light, ω the angular frequency difference of the incident and scattered light, c the velocity of light in a vacuum, R the distance from the scattered centre, φ the angle between the direction of observation and the direction of the electric

vector in the incident light, and $S(q, \omega)$ the space and time Fourier transform of the two-body correlation function $G(r, t)$ which is defined by Van Hove, where q is the wave vector corresponding to ω.

The observed intensity I_R may correspond to

$$I_R = K \int I(R, \omega)\, d\omega \tag{2}$$

where K is a constant determined by the condition of measurements. For a binary mixture, A–B, equation (2) is converted to [13, 14]

$$I_R = K'S(q) = K'\left[\langle\langle\alpha^2\rangle\rangle - \langle\langle\alpha\rangle\rangle^2 + c_A^2\alpha_A^2 a_{AA}(q) + 2c_A c_B \alpha_A \alpha_B a_{AB}(q) + c_B^2\alpha_B^2 a_{BB}(q)\right] \tag{3}$$

where c_i indicates the concentration of the constituent i in the mixture, $K' = K(N\Omega_0^4/2\pi R^2 c^4)\sin^2\varphi$, α_A and α_B are the polarizabilities α_e of A and B components, $\langle\langle\alpha\rangle\rangle$ represents $c_A\alpha_A + c_B\alpha_B$, and the a_{ij} values are the so-called Faber–Ziman structure factors [15] expressed in the form of

$$a_{ij}(q) = 1 + \int_0^\infty 4\pi r^2 \rho[g_{ij}(r) - 1]\frac{\sin(qr)}{qr}\, dr \tag{4}$$

where ρ is the number density and the g_{ij} values are the partial pair distribution functions.

Since the wavelength of the incident light is 514.5 nm, the momentum transfer q is of the order of 0.002 $Å^{-1}$. Therefore, we can discuss the Rayleigh scattering results in terms of $a_{ij}(q)$ in the long-wavelength limit as $q \to 0$. According to BT theory, $a_{ij}(0)$ values $(i, j = A, B)$ for a binary fluid mixture A–B are given by [5]

$$\begin{aligned} a_{AA}(0) &= \frac{Nk_BT}{V_M}\chi_T - \frac{c_B}{c_A} + S_{cc}(0, c_A, T)\left(\delta - \frac{1}{c_A}\right)^2 \\ a_{BB}(0) &= \frac{Nk_BT}{V_M}\chi_T - \frac{c_A}{c_B} + S_{cc}(0, c_A, T)\left(\delta + \frac{1}{c_B}\right)^2 \\ a_{AB}(0) &= \frac{Nk_BT}{V_M}\chi_T + 1 + S_{cc}(0, c_A, T)\left(\delta - \frac{1}{c_A}\right)\left(\delta + \frac{1}{c_B}\right) \end{aligned} \tag{5}$$

where V_M is the molar volume and χ_T the isothermal compressibility. $S_{cc}(0, c, T)$ and δ are given by

$$S_{cc}(0, c, T) = Nk_BT \Big/ \left(\frac{\partial^2 G}{\partial c_A^2}\right)_{p,T} = Nk_BT \Big/ \left(\frac{\partial^2 \Delta G}{\partial c_A^2}\right)_{p,T} \tag{6}$$

and

$$\delta = \frac{1}{V}\left(\frac{\partial V}{\partial c_A}\right)_{p,T} \tag{7}$$

where ΔG is the Gibbs free energy of mixing $(\Delta G \equiv G - c_A G_A^0 - (1 - c_A)G_B^0)$. Combining equations (3) and (5), we obtain the scattering intensity I_R as [14]

$$I_R = K'\langle\langle\alpha\rangle\rangle^2\left[\frac{Nk_BT}{V_M}\chi_T + S_{cc}(0, c, T)\left(\delta - \frac{\alpha_A - \alpha_B}{\langle\langle\alpha\rangle\rangle}\right)^2\right]. \tag{8}$$

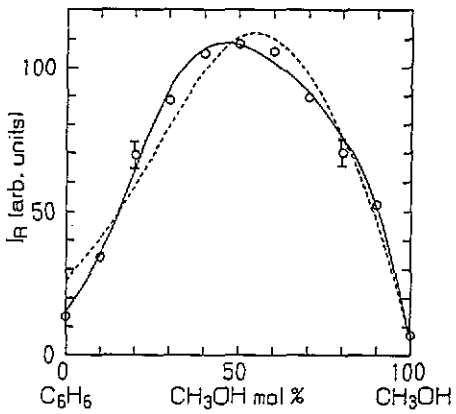

Figure 3. The Rayleigh scattering intensity of C_6H_6–CH_3OH mixtures as a function of CH_3OH concentration. The circles indicate experimental data and solid and broken lines values calculated using equation (11). For details, see text.

When there is a large difference in the molar volumes of pure components, the Gibbs free energy of mixing under the Flory approximation may be written as [16, 17]

$$\Delta G = k_B T\{c \ln \phi_A + (1-c)\ln \phi_B\} + c(1-c)\varepsilon \tag{9}$$

where ε is the regular solution parameter expressed in terms of pairwise interactions ($\varepsilon = (ZN^2/2)(2\epsilon_{12} - \epsilon_{11} - \epsilon_{22})$). The first term on the right-hand side is expressed in terms of the volume fraction ϕ of components A and B. The corresponding concentration–concentration fluctuation in the long-wavelength limit $S_{cc}(0)$ is given by

$$S_{cc}(0, c, T) = \frac{c(1-c)}{1 + c(1-c)(\delta^2 - 2\varepsilon/k_B T)} . \tag{10}$$

The application of this expression to the scattering intensities seems to be straightforward by multiplying by a constant K, which may be determined by the experimental situation, and therefore the Rayleigh scattering intensity is given by

$$I_R = K'\langle(\alpha)\rangle^2 \left[\frac{Nk_B T}{V_M}\chi_T + \frac{c(1-c)(\delta - (\alpha_A - \alpha_B)/\langle(\alpha)\rangle)^2}{1 + c(1-c)(\delta^2 - 2\varepsilon/k_B T)} \right]. \tag{11}$$

4. Results and discussion

4.1. CS_2–$CHCl_3$ and C_6H_6–CH_3OH systems

For conformal solutions of binary mixtures, the areas of Rayleigh lines of C_6H_6–CH_3OH and CS_2–$CHCl_3$ systems have been examined as shown in figures 3 and 4, respectively, by circles. As seen in the figures, the scattering intensities of the pure elements are very small and, roughly speaking, are increased until the equicomponent concentration. The increment of the scattering intensity is approximately caused by the addition of the other component into the pure system. Therefore, the net deviation in the scattering intensities from linearly interpolated values may be approximately related to the concentration fluctuations in the mixtures.

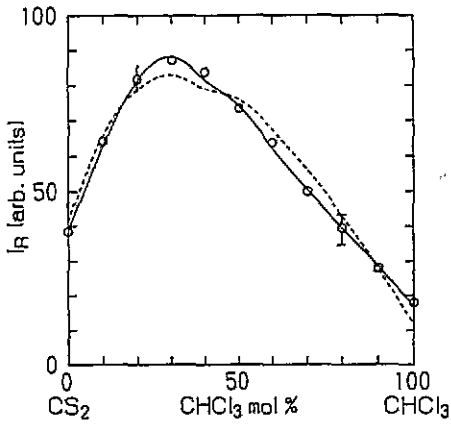

Figure 4. The Rayleigh scattering intensity of CS_2–$CHCl_3$ mixtures as a function of $CHCl_3$ concentration. The circles indicate experimental data and solid and broken lines values calculated by using equation (11). For details, see text.

Table 1. The best-fit parameters of equation (11) for the CS_2–$CHCl_3$ and C_6H_6–CH_3OH systems with the assumption that $Nk_BT\chi_T/V_M$ is a function of the concentration ratio c.

	K'	$2\varepsilon/k_BT$	$K'Nk_BT\chi_T/V_M$
C_6H_6–CH_3OH	1.34	$4.14-4.47c_{CH_3OH}$	$1.40-1.34c_{CH_3OH}$
CS_2–$CHCl_3$	14.50	$2.62-3.90c_{CHCl_3}$	$0.43-0.21c_{CHCl_3}$

By using equation (11) with the experimental data of I_R and volume data [18, 19], least-squares fitting was performed. The polarizability data used (CS_2, 8.74; $CHCl_3$, 9.5; C_6H_6, 10.32 and CH_3OH, 3.29 ($10^{-24}cm^3$)) were taken from [20]. The curves obtained are shown in figures 3 and 4 by broken lines. For the CS_2–$CHCl_3$ system, the fit between the experimental data and equation (11) is fairly good. This result implies that the mixture of CS_2 and $CHCl_3$ can be considered to be a regular solution. On the other hand, the fit for the C_6H_6–CH_3OH system is worse than that for the CS_2–$CHCl_3$ system, which suggests that the regular solution parameter ε varies with the concentration c. Therefore we try curve fitting again under the assumption that ε has the form $\varepsilon_0 + \varepsilon_1 c$. The best-fit curves are shown in figures 3 and 4 by solid lines and the parameters are listed in table 1. The agreement is excellent for both the C_6H_6–CH_3OH system and for CS_2–$CHCl_3$. Errors of the fitted parameters are less than 1% after the repeated fittings, and the criterion of the regular solution model, $2\varepsilon/k_BT < 4$, is satisfied. Therefore these two systems are exhibited in terms of a modified regular solution model. According to the literature [21], the heats of mixing for C_6H_6–CH_3OH are endothermic values at the concentrations $c_{CH_3OH} \sim 0.38$ and 0.65 and their values are 190 and 130 cal mol^{-1}, respectively. These results are, at least, consistent quantitatively and qualitatively for the concentration range from $c_{CH_3OH} = 0$–0.7. However, our results suggest that the heat of mixing turns out to be scarcely exothermic for $0.7 \leqslant c_{CH_3OH} < 1$. Although it is not easy to determine such small quantities, a direct measurement for the heat of mixing would be expected to be comparable to the present result. The concentration variation of the intermolecular interaction $2c(1-c)\varepsilon/k_BT$ is shown in figure 5, which indicates that the interaction between CS_2 and $CHCl_3$ molecules changes from repulsive on the CS_2-rich side to attractive on the $CHCl_3$-rich side. The associated complex formation is found near the concentration ratio CS_2:$CHCl_3$ = 1:4.

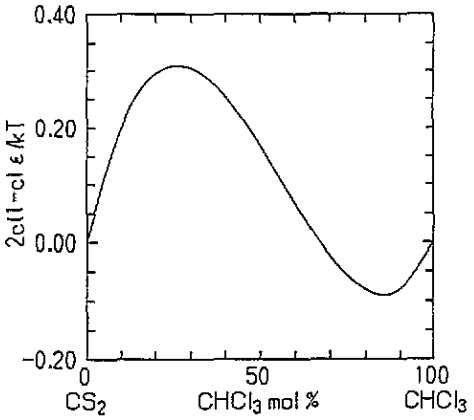

Figure 5. Interaction parameter for the CS_2–$CHCl_3$ system as a function of $CHCl_3$ concentration.

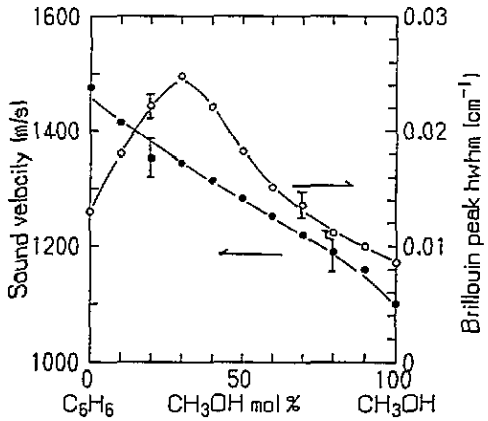

Figure 6. The sound velocity derived from the Brillouin shifts (•) and the half width of the Brillouin peak (o) in C_6H_6–CH_3OH mixtures as a function of CH_3OH concentration. Solid lines are guides for the eyes.

It is well known that the sound velocity for the systems can be derived from the Brillouin shifts. The sound velocities obtained for pure substances agree with the values in [10]. The sound velocities in C_6H_6–CH_3OH and CS_2–$CHCl_3$ systems are shown in figures 6 and 7, respectively, by filled circles. From these the adiabatic compressibilities are obtained by using a well known formula

$$\chi_S = \frac{1}{\rho v_s^2} \tag{12}$$

where ρ is the density of the system. The estimated adiabatic compressibilities for these systems are shown in figures 8 and 9, respectively, by open circles.

Under the assumption of the regular solution model, the Gibbs free energy of the system is expressed in the following form:

$$G = c_A G_A^0 + c_B G_B^0 + c_A c_B \varepsilon + k_B T(c_A \ln \phi_A + c_B \ln \phi_B). \tag{13}$$

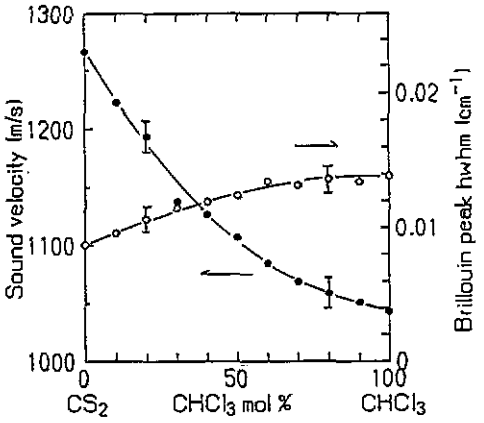

Figure 7. The sound velocity derived from the Brillouin shifts (•) and the half width of the Brillouin peak (○) in CS_2–$CHCl_3$ mixtures as a function of $CHCl_3$ concentration. Solid lines are guides for the eyes.

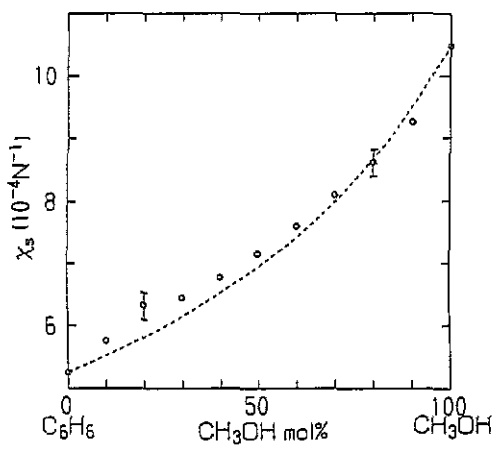

Figure 8. The adiabatic compressibilities of C_6H_6–CH_3OH mixtures as a function of CH_3OH concentration. The circles indicate the values derived from the sound velocity and the broken line is calculated using equation (17).

G_i^0 in the first two terms on the right-hand side of equation (13) are the Gibbs free energy of the pure component i and all other terms are equal to ΔG as described in equation (9).

According to thermodynamical relations, the isothermal compressibility χ_T is given by

$$\chi_T = -\frac{1}{V}\left(\frac{\partial V}{\partial p}\right)_T \tag{14}$$

and

$$V = \left(\frac{\partial G}{\partial p}\right)_{T,N} . \tag{15}$$

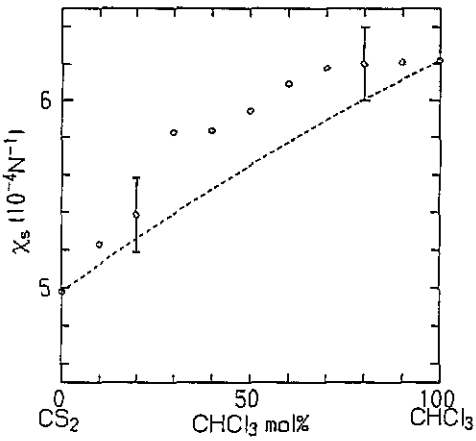

Figure 9. The adiabatic compressibilities of CS_2–$CHCl_3$ mixtures as a function of $CHCl_3$ concentration. The circles indicate the values derived from the sound velocity and the broken line is calculated by using equation (17).

If ε is a linear function of pressure and if the entropy term is nearly equal to that of an ideal mixture TS^0_{mix} ($= k_B T(c_A \ln c_A + c_B \ln c_B)$), then we have approximately

$$\chi_T \simeq \frac{c_A V_A}{V}\chi^0_{T,A} + \frac{c_B V_B}{V}\chi^0_{T,B}\,. \tag{16}$$

Therefore the concentration dependence under the assumption of the regular solution model is generally given by a convex curve. For the adiabatic compressibility, this tendency seems to be valid.

The estimated χ_s values defined as below are also plotted in figures 8 and 9 by dotted lines:

$$\chi_s \simeq \frac{c_A V_A}{V}\chi^0_{s,A} + \frac{c_B V_B}{V}\chi^0_{s,B}\,. \tag{17}$$

As seen in figure 8, for the C_6H_6–CH_3OH system χ_s satisfies the above tendency. However for the CS_2–$CHCl_3$ system (figure 9), a deviation of the observed χ_s from the values of equation (17) is seen, which is attributable to the pressure dependence of the interaction parameter ε.

The width of the Brillouin peak is related to the sound absorption. The observed half width at half maximum of the Brillouin peaks for the C_6H_6–CH_3OH and CS_2–$CHCl_3$ systems are shown in figures 6 and 7, respectively, by open circles. The half widths vary very differently for these two systems with changing concentration. The peak seen in the C_6H_6–CH_3OH system suggests that transmission of sound waves is obstructed in the C_6H_6–CH_3OH mixture. An increase in the sound-attenuation coefficient of this system may be caused by the term relating to the quantity $\partial\mu/\partial c$, where μ is the chemical potential, which contribution is well discussed in the literature (see, for example, [22]).

4.2. Fluid mixtures with a miscibility gap (CH_3OH–C_6H_{12} system)

This system has a fairly small difference between the densities of the two components and displays a miscibility gap of two phases at room temperature. In the procedure of preparing

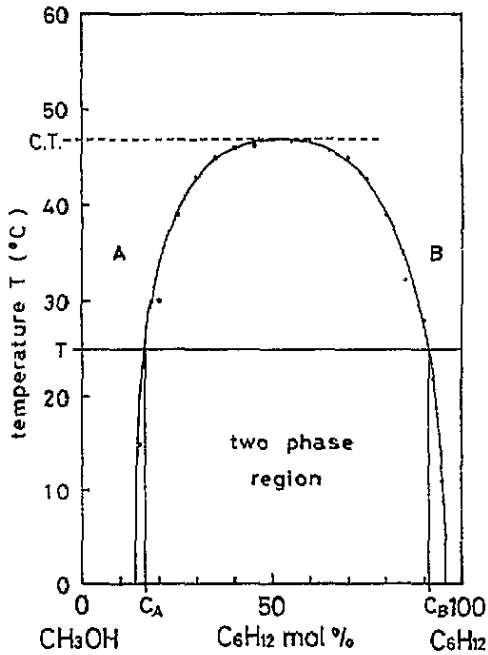

Figure 10. The phase diagram of the $_3OH$–C_6H_{12} system [23].

a sample, if their concentration ratio is given as c, even after fully shaking the container, the sample may be divided into two phases A and B as seen in figure 10 [23]. So the lower fluid must be A and the upper one is B.

In fluid A, C_6H_{12} at c_A mol% is dissolved into CH_3OH. In a similar way CH_3OH of $1 - c_B$ mol% is dissolved into C_6H_{12} in fluid B. Therefore, all samples with the nominal concentration ratio at c, if this is in the range between c_A and c_B at a given temperature T as seen in figure 10, should be separated into the two phases A and B by $(c_B - c)$ and $(c - c_A)$ respectively.

The scattering intensities have been measured for various position of the specimen container. The top and the bottom of the container correspond to 15 mm and 35 mm of beam height in figure 11, respectively. Step-wise intensities are caused by crossing from the upper phase to the lower one. These have no height dependence and the concentration dependences are shown in figure 12. Further measurements in the one-phase region and near the critical point are now in progress for several systems.

5. Summary

Light-scattering measurements have been performed for organic–organic liquid mixtures. As conformal mixtures, the CS_2–$CHCl_3$ and C_6H_6–CH_3OH systems are investigated. For these systems the Rayleigh scattering intensities and the adiabatic compressibilities derived from their Brillouin shifts are well expressed by a regular solution model with slight changes to the interaction parameter. A kind of associated complex formation is suggested near the concentration ratio CS_2:$CHCl_3$ = 1:4, where the interaction parameter has a negative maximum.

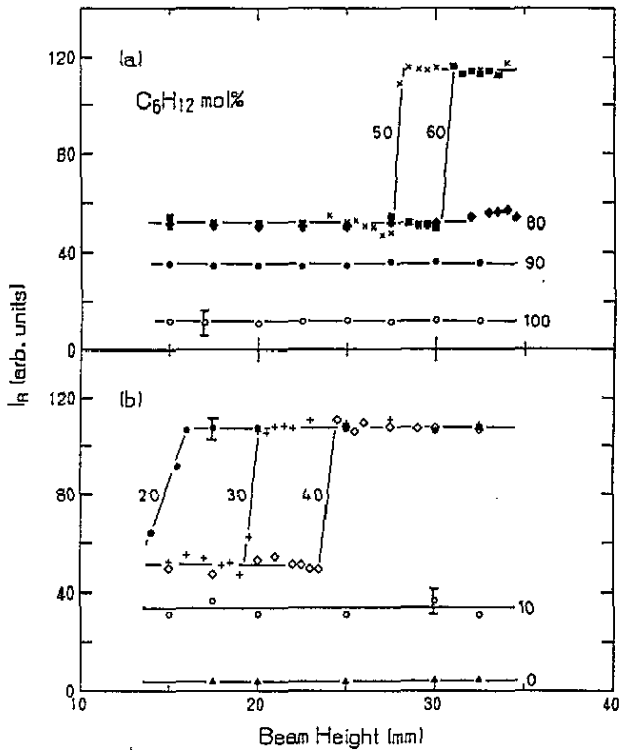

Figure 11. The observed Rayleigh scattering intensity for the CH_3OH–C_6H_{12} system as a function of light-beam height. The molar fraction of C_6H_{12} is indicated in the figure. The curves in the figure are guides for the eyes.

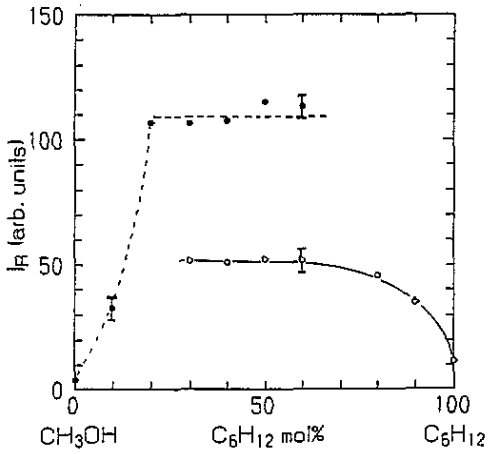

Figure 12. The Rayleigh scattering intensity near the phase interface for the CH_3OH–C_6H_{12} system as a function of the C_6H_{12} concentration. The open and full circles represent the scattering intensities in C_6H_{12}- and CH_3OH-rich phases, respectively. The solid and broken curves in the figure are guides for the eyes.

The Rayleigh scattering intensity of liquid mixtures with a miscibility gap was also

investigated. For the C_6H_{12}–CH_3OH system, the light-scattering intensity obtained was reasonable in the sense that it reproduces the exact phase diagram for all compositions.

Acknowledgment

The authors are grateful to Professor Tamaki for valuable discussion.

References

[1] Abdel-Azim A-A A and Munk P 1987 *J. Phys. Chem.* **91** 3910
[2] Oda K, Hayakawa R and Wada Y 1973 *Japan. J. Appl. Phys.* **12** 1326
[3] Mitchel R S and Guillet J E 1974 *J. Polym. Sci.* **12** 713
[4] Fiedman E A, Ritger A J and Andrews R D 1969 *J. Appl. Phys.* **40** 4232
[5] Bhatia A B and Thornton D E 1970 *Phys. Rev.* B **2** 3004
[6] Miller G A and Lee C S 1973 *J. Phys. Chem.* **77** 2441
[7] Abdel-Azim A-A A, Cheng W, El-Hibri M J and Munk P 1988 *J. Phys. Chem.* **92** 2663
[8] Cheng W, Abdel-Azim A-A A, El-Hibri M J, Du Q and Munk P 1989 *J. Phys. Chem.* **93** 8248
[9] Iwasaki K, Katayanagi Y and Fujiyama T 1976 *Bull. Chem. Soc. Japan* **49** 2988
[10] Iwasaki K, Tanaka M and Fujiyama T 1976 *Bull. Chem. Soc. Japan* **49** 2719
[11] Van Hove L 1954 *Phys. Rev.* **95** 249
[12] Komarov L I and Fisher I Z 1963 *Sov. Phys.–JETP* **16** 1358
[13] Bhatia A B and Tong E 1968 *Phys. Rev.* **173** 231
[14] Cusack N E 1987 *The Physics of Structurally Disordered Matter* (Bristol: Hilger) ch 3
[15] Faber T E and Ziman J M 1965 *Phil. Mag.* **11** 153
[16] Waseda Y, Jacob K T and Tamaki S 1984 *High Temp. Mater. Processes* **6** 119
[17] Tamaki S 1987 *Can. J. Phys.* **65** 286
[18] Brown I and Smith F 1962 *Aust. J. Chem.* **15** 1
[19] Schmidt G C 1926 *Z. Phys. Chem.* **164** 221
[20] Miller T M 1988 *Handbook of Chemistry and Physics* 6th edn, ed R C West (Boca Raton, FL: Chemical Rubber Company) p E-68
[21] *Landolt–Börnstein New Series* 1976 Group IV, vol 2, ed Beggerow (Berlin: Springer) ch 3
[22] Hansen J P and McDonald I R 1986 *Theory of Simple Liquids* (London: Academic) ch 8
[23] Kawase S, Maruyama K, Tamaki S and Okazaki H *J. Phys. Chem. Liq.* submitted